AGU PUBLICATIONS

Geophysical Research Letters

RESEARCH LETTER
10.1002/2017GL073012

Special Section:
The Arctic: An AGU Joint Special Collection

Accelerated increase in the Arctic tropospheric warming events surpassing stratospheric warming events during winter

S.-Y. Simon Wang[1,2], Yen-Heng Lin[2], Ming-Ying Lee[3], Jin-Ho Yoon[4], Jonathan D. D. Meyer[1,2], and Philip J. Rasch[5]

[1]Utah Climate Center, Utah State University, Logan, Utah, USA, [2]Department Plants, Soils and Climate, Utah State University, Logan, Utah, USA, [3]Central Weather Bureau, Taipei, Taiwan, [4]School of Earth Sciences and Environmental Engineering, Gwangju Institute of Science and Technology, Gwangju, South Korea, [5]Pacific Northwest National Laboratory, Richland, Washington, USA

Abstract In January 2016, a robust reversal of the Arctic Oscillation took place associated with a rapid tropospheric warming in the Arctic region; this was followed by the occurrence of a classic sudden stratospheric warming in March. The succession of these two distinct Arctic warming events provides a stimulating opportunity to examine their characteristics in terms of similarities and differences. Historical cases of these two types of Arctic warming were identified and validated based upon tropical linkages with the Madden-Julian Oscillation and El Niño as documented in previous studies. The analysis indicates a recent and seemingly accelerated increase in the tropospheric warming type versus a flat trend in stratospheric warming type. The shorter duration and more rapid transition of tropospheric warming events may connect to the documented increase in midlatitude weather extremes, more so than the route of stratospheric warming type. Forced simulations with an atmospheric general circulation model suggest that the reduced Arctic sea ice contributes to the observed increase in the tropospheric warming events and associated remarkable strengthening of the cold Siberian high manifest in 2016.

Plain Language Summary Rapid Arctic warming events disrupt mid-latitude weather patterns and oftentimes produce extreme deviations from normal weather conditions. The atmospheric origins of these Arctic warming events have been identified as developing in the troposphere and the stratosphere. Using historical observations, we have found that the frequency of tropospheric warming events has increased through the recent decades, while the stratospheric events have not. We have also found that tropospheric events develop twice as fast as stratospheric events and are therefore less predictable. With observations of historically-low Arctic sea ice extent occurring alongside the increase of tropospheric warming events, computer simulations provided evidence that the two phenomena are likely linked. Along with observational evidence for enhanced transport of tropical energy helping fuel these Arctic tropospheric warming events, these results suggest that future mid-latitude weather is likely to undergo an increase to extreme, unseasonal weather patterns that are inherently less predictable.

Key Points:
- A distinct type of Arctic warming events is identified, one that is confined in the troposphere without a stratospheric precursor
- Tropospheric warming events occur twice as fast as the stratospheric type, challenging subseasonal prediction
- Tropospheric warming events have increased at an accelerated pace, surpassing stratospheric warming events in the recent decade

Supporting Information:
- Supporting Information S1

Correspondence to:
S.-Y. S. Wang,
simon.wang@usu.edu

Citation:
Wang, S.-Y. S., Y.-H. Lin, M.-Y. Lee, J.-H. Yoon, J. D. D. Meyer, and P. J. Rasch (2017), Accelerated increase in the Arctic tropospheric warming events surpassing stratospheric warming events during winter, *Geophys. Res. Lett.*, *44*, 3806–3815, doi:10.1002/2017GL073012.

Received 8 FEB 2017
Accepted 20 MAR 2017
Accepted article online 23 MAR 2017
Published online 22 APR 2017

1. Introduction

In January 2016, the Arctic Oscillation (AO) index underwent a drastic phase reversal (Figure 1a) with excursions exceeding positive 2 standard deviations (σ) transitioning to negative 2σ within 20 days. Vertical profiles of the polar cap height (PCH) anomalies in Figure 1b, referencing the standardized geopotential height (HGT) averaged north of 65°N [e.g., *Kim et al.*, 2014], and the Arctic air temperature anomalies from long-term mean (Figure 1c) both show that the troposphere warmed and expanded rapidly in the first half of January. The upper tropospheric flows transitioned correspondingly from a zonal pattern in December to high-amplitude semistationary waves (Figure S1 in the supporting information), accompanied by extreme weather events worldwide including severe flooding in the UK and Ireland (early January), Winter Storm Jonas that "rivals biggest East Coast snowstorms on record" [*The Weather Channel*, 2016], and a tremendous buildup of the Siberian high (late January; Figure S1) leading to record cold spells in Taiwan with unprecedented 84 hyperthermia fatalities and massive agricultural damages [*TIME*, 2016]. However, operational multimodel ensemble models did not predict the widespread cold temperature anomalies across northern Europe and Eurasia even at zero-month lead (Figure S2), presenting a challenge in medium range and subseasonal prediction.

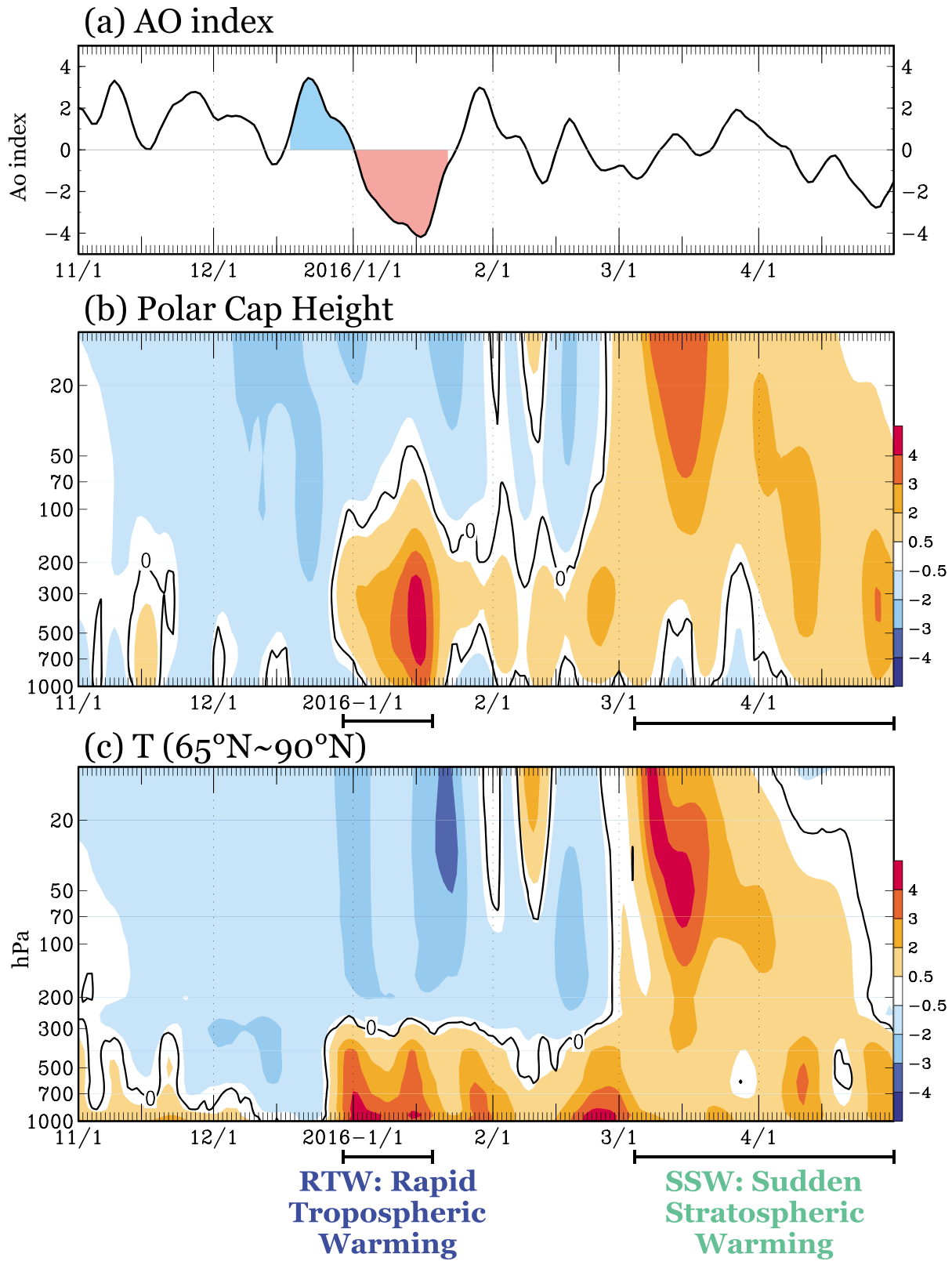

Figure 1. (a) Daily Arctic Oscillation index from 1 November to 30 April with 5 day moving average; the shaded period indicates the rapid tropospheric warming (RTW) case. (b) Time-height cross section of daily polar cap height (PCH) over Arctic region (north of 65°N) with 5 day moving average using R2 data. (c) Same as Figure 1b but for air temperature anomaly.

This January 2016 event, referred herein as the rapid tropospheric warming (RTW), is distinct from the well-known sudden stratospheric warming (SSW) that propagates downward [*Limpasuvan et al.*, 2004; *Butler et al.*, 2015], of which a classic example was observed closely following the RTW during March and April (Figure 1). It is known that SSW acts as a precursor to AO phase change through downward propagation of the stratospheric polar vortex variation [*Baldwin and Dunkerton*, 1999; *Tripathi et al.*, 2015], though this process was not observed in the January RTW. A weakened polar vortex (negative AO) induces more cold air outbreaks [*Thompson and Wallace*, 1998] and cold surges in Asia [*Park et al.*, 2011], and strong negative AO events produce colder-than-normal winters throughout the Northern Hemisphere [*Honda et al.*, 2009; *Cohen et al.*, 2010; *L'Heureux et al.*, 2010; *Park et al.*, 2011; *Kug et al.*, 2015]. Since AO can be amplified by sea ice fluctuations [*Wang and Ikeda*, 2000; *Rigor et al.*, 2002; *Overland and Wang*, 2005], the 2016 RTW and SSW events did coincide alongside record warmth and low sea ice concentration (SIC) in the Arctic that lasted through spring [*Overland and Wang*, 2016]. The effect of Arctic warming and sea ice loss on the change in midlatitude weather extremes has been an area of active research as was reviewed by *Overland et al.* [2016], *Screen* [2017], and *Cohen et al.* [2014]. To understand the differences and the long-term changes between SSW and the reported RTW, we decided to examine their characteristics in terms of similarities and differences by using reanalysis data and a global climate model.

2. Data and Model Experiments

Daily variables derived from the National Centers for Environmental Prediction (NCEP)/Department of Energy Reanalysis II (R2) data [*Kanamitsu et al.*, 2002] and the NCEP/National Center for Atmospheric Research Reanalysis data [*Kalnay et al.*, 1996] were used for the analysis of post-1979 and post-1950 atmospheric variations, respectively. The sea surface temperature (SST) data were obtained from the Extended Range SST version 3 and the SIC data from the NOAA Optimum Interpolation SST and Sea Ice version 2 [*Reynolds et al.*, 2007]. The AO index was obtained from the NOAA Climate Prediction Center.

We conducted atmospheric general circulation experiments by using the European Centre Hamburg Atmosphere Model version 5 (ECHAM5) [*Roeckner et al.*, 2003], with T42 horizontal resolution and 31 vertical sigma levels. All simulations used initial and boundary conditions from the R2 reanalysis. Following the model setup described in *Lee et al.* [2015], the control simulation was driven by the observed climatological monthly SST and SIC (over the 1998–2010 period) while two experiments were performed. One set of simulations denoted as the SST experiment combined monthly varying SST (differing for every month and year) with climatological SIC (constant for each month and year). A second set of simulations denoted as the SIC experiment inverts the forcing, with climatological SST combined with monthly varying SIC boundary conditions. Each experiment included 30 member simulations from October to March. Text S1 in the supporting information further describes this model and its simulation setup and discusses its performance with a reference to *Saha et al.* [2014].

3. Analysis and Results

3.1. Case Identification and Composite

We first begin with an analysis of the observations to identify historical RTW events. These events require three conditions be met with the following: (1) positive PCH/HGT anomaly north of 65 N only happens in the troposphere (beneath 200 hPa), (2) PCH/HGT anomaly has a magnitude greater than 1.5σ, (3) PCH anomalies in the stratosphere remain neutral to negative, and (4) a corresponding AO phase reversal must be present to reflect the surface climate anomaly; however, the magnitude of AO was not considered. To reduce high-frequency weather signals, a 5 day moving average was applied to the PCH and the AO. Stratospheric warming (positive PCH at 70 hPa and above) must not be present both during the tropospheric warming episode and in the 15 days leading up to it (as was the case in the January 2016 RTW). We used an established definition for the SSW [*Limpasuvan et al.*, 2004; *Charlton and Polvani*, 2007; *Butler et al.*, 2015]: (1) the 50 hPa PCH with its 5 day running mean reaches an anomaly greater than 1.5σ, (2) this increased PCH then propagates downward below 200 hPa, and (3) the duration of any given event is determined by the timespan between the first appearance of warming in the stratosphere and the last appearance of warming below 200 hPa. The case selection was conducted manually; each identified case is dated in Table 1 with 30 RTW

Table 1. The Dates of Phase 1 Through Phase 7 of the Identified Cases

Case	RTW Cases: Phases 1–7	SSW Cases: Phases 1–7
1	23 Dec 1979 to 23 Jan 1980	19 Feb 1980 to 26 Mar 1980
2	8 Jan 1983 to 6 Feb 1983	2 Feb 1981 to 7 Mar 1981
3	12 Nov 1985 to 25 Nov 1985	2 Dec 1981 to 30 Dec 1981
4	18 Jan 1986 to 30 Jan 1986	1 Mar 1983 to 29 Mar 1983
5	16 Jan 1988 to 4 Feb 1988	26 Dec 1983 to 13 Mar 1984
6	10 Feb 1988 to 27 Feb 1988	9 Dec 1984 to 19 Jan 1985
7	26 Dec 1990 to 12 Jan 1991	17 Jan 1987 to 21 Mar 1987
8	24 Nov 1991 to 3 Dec 1991	10 Nov 1987 to 23 Dec 1987
9	31 Jan 1994 to 24 Feb 1994	4 Feb 1989 to 16 Mar 1989
10	28 Feb 1995 to 10 Mar 1995	25 Jan 1991 to 9 Mar 1991
11	21 Feb 1996 to 16 Mar 1996	17 Dec 1991 to 16 Feb 1992
12	28 Feb 1997 to 20 Mar 1997	9 Nov 1993 to 10 Jan 1994
13	5 Feb 2000 to 17 Feb 2000	22 Dec 1994 to 28 Jan 1995
14	27 Feb 2000 to 16 Mar 2000	7 Nov 1996 to 30 Dec 1996
15	11 Nov 2001 to 7 Dec 2001	9 Dec 1997 to 10 Jan 1998
16	18 Nov 2002 to 7 Dec 2002	10 Dec 1998 to 11 Jan 1999
17	5 Jan 2005 to 26 Jan 2005	25 Jan 1999 to 10 Mar 1999
18	9 Feb 2005 to 26 Feb 2005	25 Nov 2000 to 28 Dec 2000
19	8 Nov 2006 to 24 Nov 2006	24 Jan 2001 to 24 Mar 2001
20	19 Jan 2007 to 7 Feb 2007	15 Feb 2002 to 23 Mar 2002
21	18 Nov 2008 to 30 Nov 2008	24 Nov 2003 to 16 Jan 2004
22	15 Nov 2010 to 26 Nov 2010	10 Jan 2006 to 21 Mar 2006
23	2 Dec 2010 to 17 Dec 2010	21 Feb 2008 to 29 Mar 2008
24	27 Dec 2010 to 10 Jan 2011	10 Jan 2009 to 13 Feb 2009
25	14 Nov 2012 to 29 Nov 2012	2 Nov 2009 to 4 Jan 2010
26	16 Dec 2013 to 5 Jan 2014	17 Jan 2010 to 23 Feb 2010
27	10 Jan 2014 to 28 Jan 2014	24 Dec 2011 to 28 Jan 2012
28	10 Feb 2014 to 28 Feb 2014	9 Jan 2013 to 20 Mar 2013
29	3 Nov 2014 to 13 Nov 2014	
30	17 Feb 2016 to 4 Mar 2016	
2015-16[a]	22 Dec 2015 to 15 Jan 2016	13 May 2016 to 27 Apr 2016

[a]Not used in the composite. The period of 2015–2016 shows the date of the recent extreme cases that are included in the composite analysis.

and 28 SSW cases. For the reader's reference, each year's observed PCH profiles during the 1950–2016 period are shown in Figure S3.

To depict the common characteristics within a given AO/RTW episode, we adopted the "index cycle" approach of the AO that aligns the same phase of each oscillation episode, following *Tanaka and Tokinaga* [2002] and *Wang et al.* [2014]. The transition from positive to negative status was evenly divided into seven phases: phase 1 designates the maximum AO, and phase 7 represents the minimum AO, each phase comprising 5 days centered on the third day. We then constructed the composites of the vertical PCH profiles, air temperature anomalies, and corresponding AO indices; these are shown in Figure 2 (the 2016 case was removed from the composite for the "leave one out" verification). It was found that the average AO transition in SSW takes an average of 48 days ± 15 days (1σ), more than twice as long than RTW that averaged 19 days (±5 days); these are also shown in Figure 2. (In Figure 2 and ensuing composite analysis, significance level was computed based on Student's *t* test.)

Next, the dynamical aspects of RTW and SSW were compared with the previous observations of the tropical intraseasonal variations. One of the documented variation modes that can modulate the Arctic temperature and AO is the Madden-Julian Oscillation (MJO) [*L'Heureux and Higgins*, 2008; *Yoo et al.*, 2012; *Goss et al.*, 2016]. Figure 3a shows the 250 hPa velocity potential (VP) during the 2016 RTW event, which reveals a zonal wave-1 structure of VP that apparently propagated eastward up to phase 6. Such a wave-1 pattern and its eastward propagating signal are indicative of an MJO, of which a strong event occurred during January 2016 (http://www.bom.gov.au/climate/mjo/). In the RTW composite (Figure 3b), the VP propagation is even more pronounced and is phase-consistent with the 2016 case. In the SSW composite (Figure 3c), the VP pattern is rather disorganized and weak, suggesting minimal MJO influence. The analysis of the 250 hPa streamfunction (Figure S4) outlines the corresponding stationary wave anomalies with the 2016 case, in which a Pacific-North America (PNA) type of teleconnection pattern can be seen.

We further computed the Eliassen-Palm Flux [*Edmon et al.*, 1980] and plotted the zonal-mean eddy momentum component with latitude in Figure 3, denoted as EPF. A zonally averaged EPF diagnoses the impact of transient eddies on the time mean flow and, in turn, delineates the large-scale and fast responses in the planetary wave trains that connect between the tropics and the Arctic [*Trenberth*, 1986]. As shown in Figure 3 (right axis of each panel) by the positive EPF that persisted throughout phases 3–7, RTW is more pronouncedly affected by tropical teleconnections; in contrast, positive EPF in SSW only is present in phases 6 and 7. This result is in good agreement with the corresponding streamfunction anomalies in Figure S4 showing a larger amplitude of the midlatitude stationary waves in the RTW composite, as well as the previous studies that identified the MJO influence on heat and moisture fluxes into the Arctic [*Yoo et al.*, 2012; *Park et al.*, 2015].

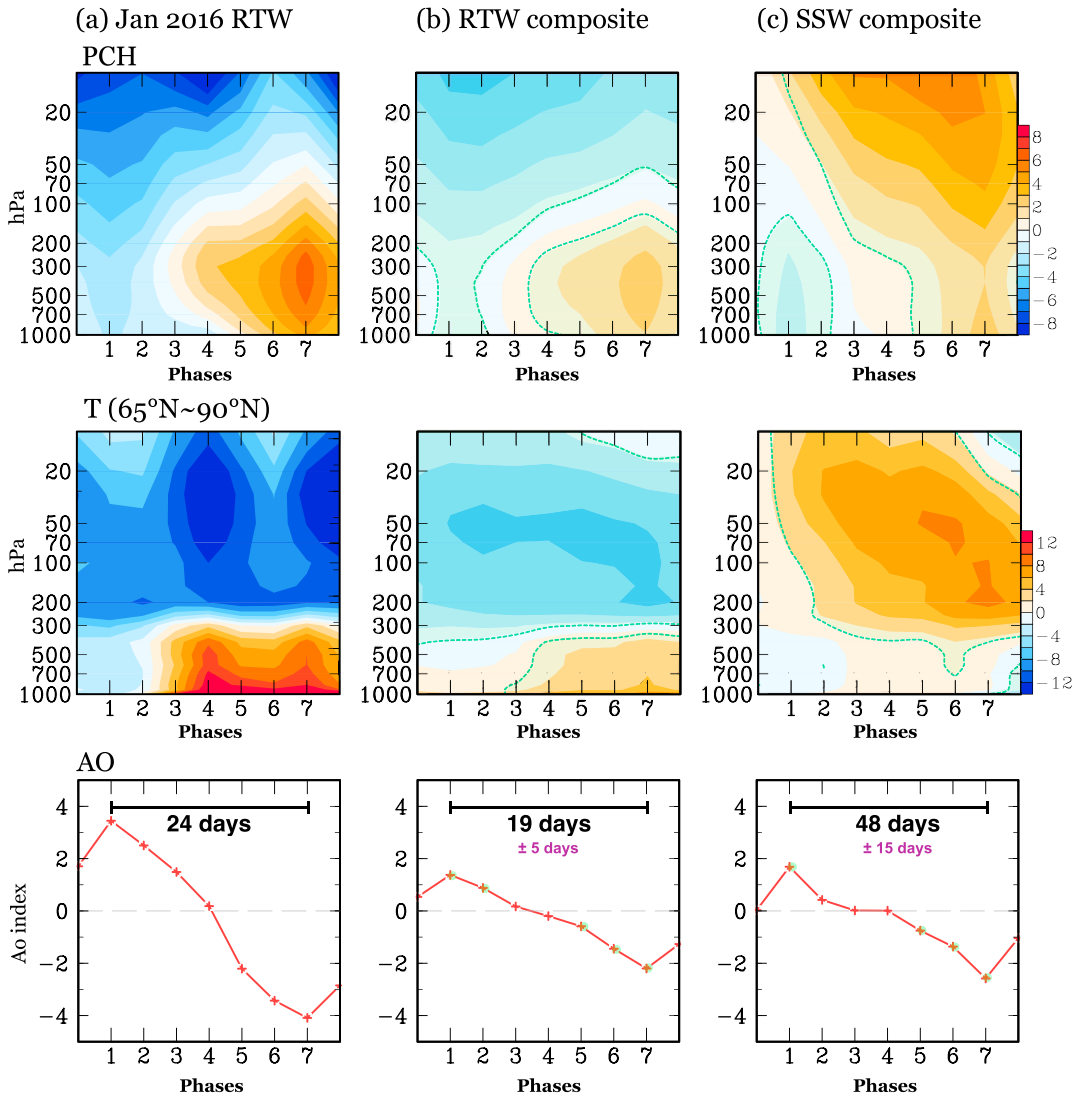

Figure 2. (top) Composite PCH and (middle) air temperature spanning the seven phases of the index cycle (see text) averaged north of 65°N and (bottom) corresponding AO index for (a) the January 2016 RTW case, (b) composite RTW with 30 cases, and (c) composite SSW with 28 cases since 1979, using R2 data. The averaged duration and 1 standard deviation (purple) of total cases are labeled, and the phases representing 0 and 8 were derived from 4 day averages before 1 and after 7, respectively. The green dashed lines in Figures 2b and 2c outline 95% confidence interval for the *t* distribution.

3.2. Disparity in the Trends

Encouraged by the consistency between the composite RTW and the January 2016 case presented in Figure 2, we proceeded to examine the long-term frequencies of cases beginning in 1953, with a 9 year interval (that allows for equal number of years up to 2016. As shown in Figure 4a, the frequency of RTW underwent a marked increase since the 1990s, more than doubled in the last decade, while the SSW frequency reveals a flat trend. The number of the RTW cases appears to exceed that of the SSW cases in the recent decade (though the exact numbers are likely dependent on the event definition). This marked increase in RTW may signify the emergence of the disproportionate Arctic warming (relative to midlatitudes) from the noise of natural variability since the late 1990s [*Serreze et al.*, 2009]. However, the increase in frequency should not reflect the Arctic warming, since the daily long-term trends of PCH and AO have been removed in the case selection.

To illustrate the frequency changes of RTW and SSW, Figures 4b and 4c show the daily distribution of extreme Arctic temperature anomalies from the 50 hPa level and the 1000–500 hPa average, respectively, during

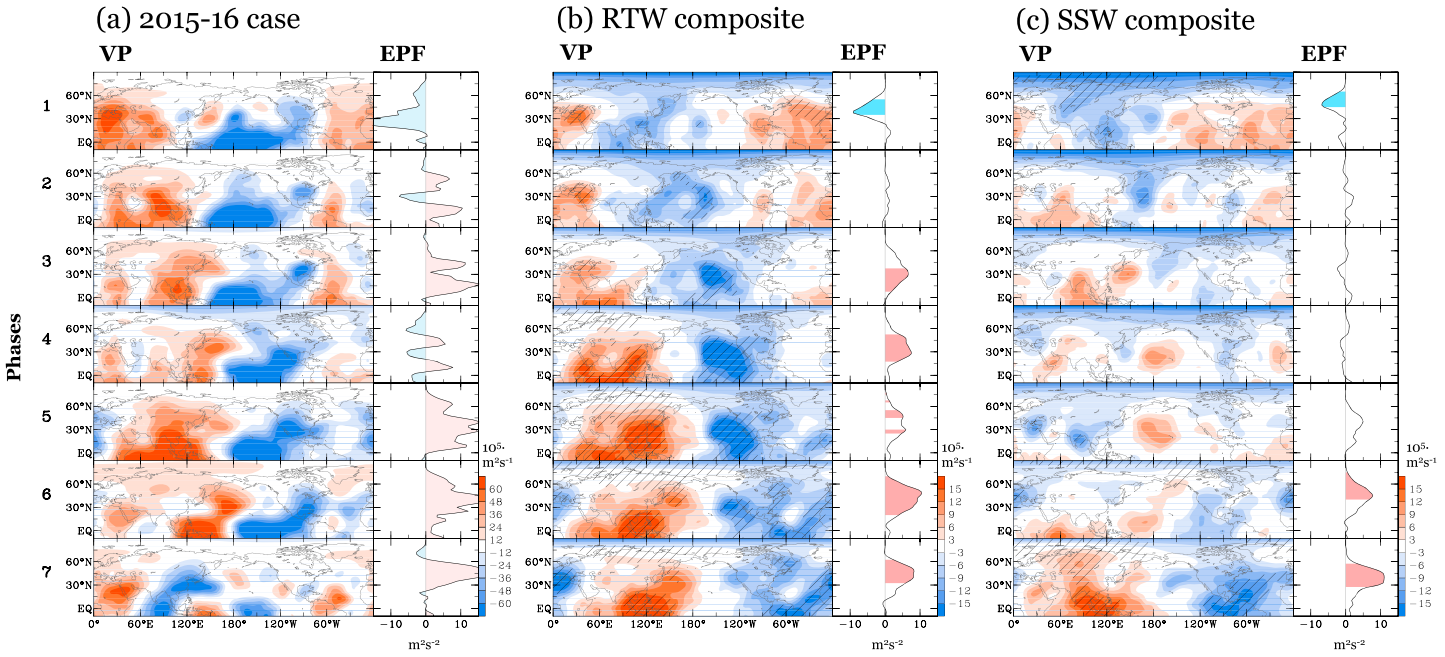

Figure 3. Composite seven phases of 250 hPa velocity potential (VP) and the eddy momentum component of the E-P flux (EPF) computed from (a) the January 2016 RTW case, (b) historical RTW cases, and (c) historical SSW cases. Hatched areas of VP and shaded areas of EPF in Figures 3b and 3c signify 95% confidence interval for the *t* distribution.

November–March starting in 1979 (using R2, with the daily long-term trend removed). The daily temperature thresholds used for the depiction of extreme warming are indicated in the legend. It is apparent that only the occurrence of tropospheric warming has increased and the cluster of changes has taken place in the beginning of the 21st century.

3.3. Impact of External Forcing

The concurrence of the January 2016 RTW event with the strong El Niño led to a speculation concerning the extent to which tropical sea surface temperature anomalies affect the Arctic warming. Previous studies [*Ineson and Scaife*, 2009; *Butler et al.*, 2014; *Johnson and Kosaka*, 2016] have identified a stratospheric pathway from which El Niño affects the Arctic circulation and temperature. However, the January 2016 RTW case was not preceded by any stratospheric warming (Figure 1) and, as was stated in *Overland and Wang* [2016], the 2016 El Niño did not contribute to the AO change. Hence, we show in Figures 5a and 5b the differences in the January sea level pressure (SLP) of the SIC experiment and the SST experiment from the control experiment to assess their respective role. The corresponding T anomalies are shown in Figure S5. The SLP patterns in the two experiments are apparently opposite over Eurasia and Siberia, where the impact from SIC anomalies in the Barents-Kara (B-K) Seas is known to be pronounced [*Inoue et al.*, 2012; *Park et al.*, 2015]. Compared with the 2016 anomaly (Figure 5c), the SIC experiment produced a similar SLP pattern in Eurasia and Siberia, while the SST experiment captured the classic Pacific-North America (PNA) teleconnection. Given the short duration of RTW (~20 days), PCH anomalies in the troposphere may reflect synoptic or intraseasonal variability more than a modulation of annular mode by some external forcings [*Löptien and Ruprecht*, 2005]. In the case of January 2016, a series of intense North Atlantic storms did contribute to the Arctic warming [*Kim et al.*, 2017]. In terms of air temperature, SIC experiment led to substantial cooling in Siberia, while SST experiment generated a pan-Arctic cooling instead (Figure S5). Additional examination of the intraseasonal variations, shown in Text S2 and Figure S6 in the supporting information, suggests that SIC reduction can amplify intraseasonal variability in the Arctic region.

To more quantitatively describe the pattern difference between SIC and SST experiments, we computed the sliding spatial correlation between the experiments and observed 2016 anomaly, with a circumglobal 180° longitude range (from 35°N to 90°N centered at the longitude of *x* axis). As shown in Figure 5e, the sliding correlations delineate an opposite response from the two experiments, where the SST experiment produced a PNA-like response in the western hemisphere primarily in North America, while the SIC experiment

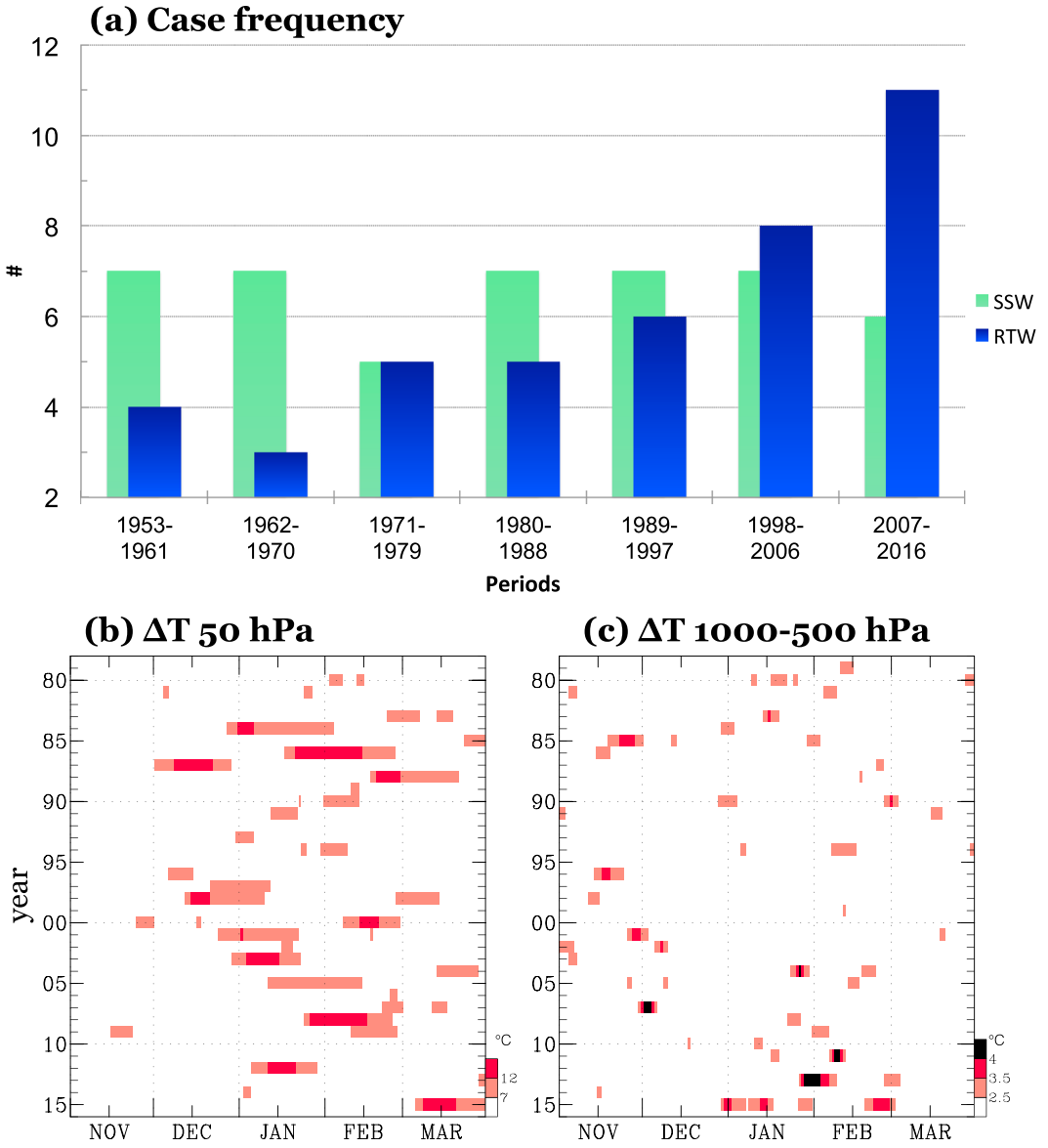

Figure 4. (a) The case frequencies of RTW (blue) and SSW (light green) cases plotted at every 9 years during the November–March period and occurrence of Arctic region (north of 65°N) temperature anomalies with the daily long-term mean removed at (b) 50 hPa and (c) 1000–500 hPa average exceeding the color-coded thresholds.

generates a response in the eastern hemisphere encompassing Siberia end Eurasia. The SIC experiment produced the documented connection of the B-K Seas' low sea ice with Siberia's abnormally cold winters [*Honda et al.*, 2009; *Petoukhov and Semenov*, 2010; *Kim et al.*, 2014]. Moreover, the SIC decline in 2016 apparently led to a high-pressure response over Siberia, and this corresponds to the post-1979 trend in SLP (Figure 5d), a change that was driven by sea ice loss [*Screen and Simmonds*, 2013; *Vihma*, 2014]. However, we did not observe any upward propagation of eddy heat flux into the stratosphere during the January 2016 RTW (not shown).

Butler et al. [2014] have indicated that El Niño can increase temperature in high-latitude North America through a tropospheric pathway; here the SST experiment produced a marked Arctic cooling instead (Figure S5). As a further examination, the sliding spatial correlation between the two experiments and the observed SLP trends (Figure 5f) shows that SLP trends in the Arctic region and Siberia are highly correlated with SLP anomalies in both the SIC experiment and January 2016 anomaly, suggesting that El Niño's effect on the Arctic circulations was largely offset by that of SIC reduction over the eastern hemisphere and Siberia in 2016.

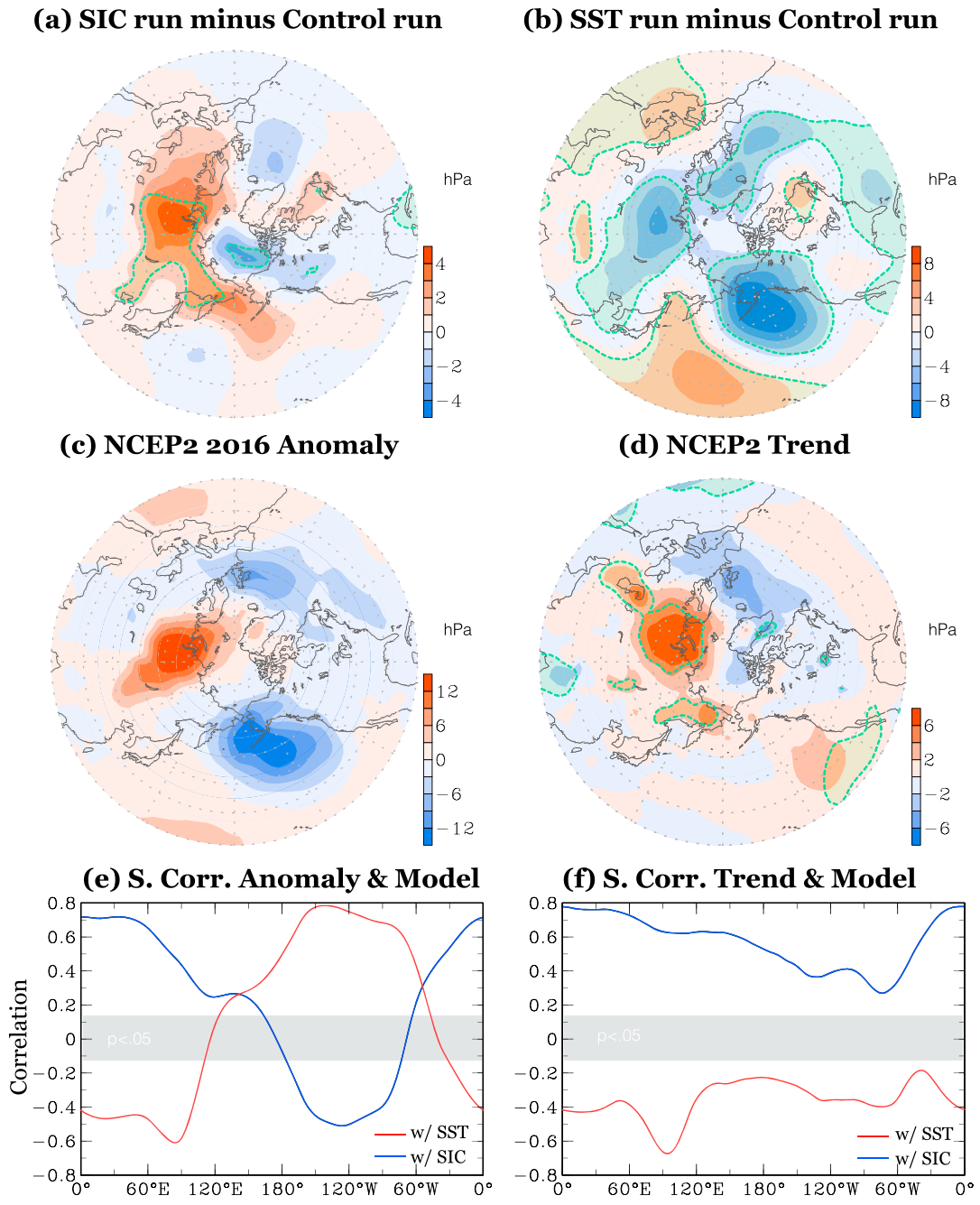

Figure 5. Ensemble mean of the January sea level pressure (SLP) anomalies simulated by (a) SIC run and (b) SST run subtracted from control run. (c) January 2016 SLP anomaly derived from R2. (d) Linear trends in SLP from 1979 to 2016 multiplied by 37 years by using R2; the green contours indicate 95% confidence interval for the *t* distribution. The sliding spatial correlation over 35°N–90°N with an 180° longitude range centered at the *x* axis value (i.e., 90° to the west and 90° to the east) between (e) the 2016 anomaly and the two ECHAM5 runs and (f) the post-1979 linear trend and the two runs.

4. Conclusions

This study was motivated by the observation of two distinct Arctic warming events occurring in succession during early 2016, one confined in the troposphere with a shorter duration (RTW) and the other being a classic SSW with a longer time span. Given the high-impact consequence of the January 2016 RTW and the challenge it presented to subseasonal prediction (Figure S2), their differences and frequencies were examined. Composite analysis based on PCH and AO criteria was compared with those documented in the

literature, including tropical influence, ENSO impact, and SIC effects. Subsequent analysis uncovered distinct trends in the frequencies of RTW and SSW events: whereas the frequency of SSW has not changed in any significant way, the frequency of RTW has increased dramatically and appears to accelerate since the 1990s, surpassing SSW events in the recent decade. Forced experiments using ECHAM5 indicated that the loss of sea ice (as was the case during 2016's record low SIC) can amplify intraseasonal variations in the high-latitude circulations which, according to the literature [*Harnack and Crane*, 1984; *Horel and Mechoso*, 1988; *Athanasiadis et al.*, 2014], can translate to increased atmospheric blocking during winter season and subsequent cold surges. These results are substantial in that RTW and associated fast AO transition involve more pronounced influxes of Rossby wave energy and moisture from the tropics than of SSW; this further suggests an increased risk of cold-season extreme weather events accompanying RTW.

Recent studies have unequivocally indicated that the loss of sea ice profoundly influences temperatures and circulations over the Arctic region which, in turn, modulates the midlatitude extreme weather [*Cohen et al.*, 2014; *Jung et al.*, 2014; *Kug et al.*, 2015]. This study moves one step further by highlighting the existence of, and the increase in, the RTW type of Arctic events that may possess a greater threat in the form of midlatitude extreme weather. Future work requires high-resolution modeling to properly represent regional dynamic processes revealed in the 2016 RTW and SSW cases and predict similar cases beyond weather forecasting timescale.

Acknowledgments
The research is supported by grant DE-SC0016605 and the Utah Agricultural Experiment Station, Utah State University (paper #8980), with partial support from the Central Weather Bureau of Taiwan. J.H. Yoon was supported by the "Climate Technology Development and Application" research project (K07743) through a grant provided by GIST in 2017. P.J.R. was supported by the U.S. Department of Energy Office of Science, Biological and Environmental Research (BER) program as part of the Regional and Global Climate Modeling (RGCM) project. Observational and reanalysis data used in this study are provided by the NOAA/OAR/ESRL PSD, Boulder, Colorado, from their website at http://www.esrl.noaa.gov/psd/.

References

Athanasiadis, P. J., A. Bellucci, L. Hermanson, A. A. Scaife, C. MacLachlan, A. Arribas, S. Materia, A. Borrelli, and S. Gualdi (2014), The representation of atmospheric blocking and the associated low-frequency variability in two seasonal prediction systems, *J. Clim.*, *27*(24), 9082–9100.

Baldwin, M. P., and T. J. Dunkerton (1999), Propagation of the Arctic Oscillation from the stratosphere to the troposphere, *J. Geophys. Res.*, *104*, 30,937–30,946, doi:10.1029/1999JD900445.

Butler, A. H., L. M. Polvani, and C. Deser (2014), Separating the stratospheric and tropospheric pathways of El Niño–Southern Oscillation teleconnections, *Environ. Res. Lett.*, *9*(2), 024,014.

Butler, A. H., D. J. Seidel, S. C. Hardiman, N. Butchart, T. Birner, and A. Match (2015), Defining sudden stratospheric warmings, *Bull. Am. Meteorol. Soc.*, *96*(11), 1913–1928.

Charlton, A. J., and L. M. Polvani (2007), A new look at stratospheric sudden warmings. Part I: Climatology and modeling benchmarks, *J. Clim.*, *20*(3), 449–469.

Cohen, J., J. Foster, M. Barlow, K. Saito, and J. Jones (2010), Winter 2009–2010: A case study of an extreme Arctic Oscillation event, *Geophy. Res. Lett.*, *37*, L17707, doi:10.1029/2010GL044256.

Cohen, J., J. A. Screen, J. C. Furtado, M. Barlow, D. Whittleston, D. Coumou, J. Francis, K. Dethloff, D. Entekhabi, and J. Overland (2014), Recent Arctic amplification and extreme mid-latitude weather, *Nat. Geosci.*, *7*(9), 627–637.

Edmon, H., Jr., B. Hoskins, and M. McIntyre (1980), Eliassen-Palm cross sections for the troposphere, *J. Atmos. Sci.*, *37*(12), 2600–2616.

Goss, M., S. B. Feldstein, and S. Lee (2016), Stationary wave interference and its relation to tropical convection and arctic warming, *J. Clim.*, *29*(4), 1369–1389.

Harnack, R. P., and M. W. Crane (1984), Intraseasonal tropospheric circulation variability and its association with concurrent atmospheric and oceanic fields, *Mon. Weather Rev.*, *112*(9), 1768–1781.

Honda, M., J. Inoue, and S. Yamane (2009), Influence of low Arctic sea-ice minima on anomalously cold Eurasian winters, *Geophy. Res. Lett.*, *36*, L08707, doi:10.1029/2008GL037079.

Horel, J. D., and C. R. Mechoso (1988), Observed and simulated intraseasonal variability of the wintertime planetary circulation, *J. Clim.*, *1*(6), 582–599.

Ineson, S., and A. Scaife (2009), The role of the stratosphere in the European climate response to El Niño, *Nat. Geosci.*, *2*(1), 32–36.

Inoue, J., M. E. Hori, and K. Takaya (2012), The role of Barents Sea ice in the wintertime cyclone track and emergence of a warm-Arctic cold-Siberian anomaly, *J. Clim.*, *25*(7), 2561–2568.

Johnson, N. C., and Y. Kosaka (2016), The impact of eastern equatorial Pacific convection on the diversity of boreal winter El Niño teleconnection patterns, *Clim. Dyn.*, *47*, 3737–3765.

Jung, T., M. A. Kasper, T. Semmler, and S. Serrar (2014), Arctic influence on subseasonal midlatitude prediction, *Geophy. Res. Lett.*, *41*, 3676–3680, doi:10.1002/2014GL059961.

Kalnay, E., et al. (1996), The NCEP/NCAR 40-Year Reanalysis Project, *Bull. Am. Meteorol. Soc.*, *77*(3), 437–471.

Kanamitsu, M., W. Ebisuzaki, J. Woollen, S.-K. Yang, J. J. Hnilo, M. Fiorino, and G. L. Potter (2002), NCEP-DOE AMIP-II Reanalysis (R-2), *Bull. Am. Meteorol. Soc.*, *83*(11), 1631–1643.

Kim, B.-M., S.-W. Son, S.-K. Min, J.-H. Jeong, S.-J. Kim, X. Zhang, T. Shim, and J.-H. Yoon (2014), Weakening of the stratospheric polar vortex by Arctic sea-ice loss, *Nat. Commun.*, *5*, doi:10.1038/ncomms5646.

Kim, B.-M., J.-Y. Hong, S.-Y. Jun, X. Zhang, H. Kwon, S.-J. Kim, J.-H. Kim, S.-W. Kim, and H.-K. Kim (2017), Major cause of unprecedented Arctic warming in January 2016: Critical role of an Atlantic windstorm, *Sci. Rep.*, *7*, 40051.

Kug, J.-S., J.-H. Jeong, Y.-S. Jang, B.-M. Kim, C. K. Folland, S.-K. Min, and S.-W. Son (2015), Two distinct influences of Arctic warming on cold winters over North America and East Asia, *Nat. Geosci.*, *8*(10), 759–762.

Lee, M. Y., C. C. Hong, and H. H. Hsu (2015), Compounding effects of warm sea surface temperature and reduced sea ice on the extreme circulation over the extratropical North Pacific and North America during the 2013–2014 boreal winter, *Geophy. Res. Lett.*, *42*, 1612–1618, doi:10.1002/2014GL062956.

L'Heureux, M. L., and R. W. Higgins (2008), Boreal winter links between the Madden-Julian oscillation and the Arctic Oscillation, *J. Clim.*, *21*(12), 3040–3050.

L'Heureux, M. L., A. Butler, B. Jha, A. Kumar, and W. Wang (2010), Unusual extremes in the negative phase of the Arctic Oscillation during 2009, *Geophy. Res. Lett.*, *37*, L10704, doi:10.1029/2010GL043338.
Limpasuvan, V., D. W. Thompson, and D. L. Hartmann (2004), The life cycle of the Northern Hemisphere sudden stratospheric warmings, *J. Clim.*, *17*(13), 2584–2596.
Löptien, U., and E. Ruprecht (2005), Effect of synoptic systems on the variability of the North Atlantic Oscillation, *Mon. Weather Rev.*, *133*(10), 2894–2904.
Overland, J., and M. Wang (2005), The Arctic climate paradox: The recent decrease of the Arctic Oscillation, *Geophy. Res. Lett.*, *32*, L06701, doi:10.1029/2004GL021752.
Overland, J., and M. Wang (2016), Recent extreme Arctic temperatures are due to a split polar vortex, *J. Clim.*, *29*(15), 5609–5616.
Overland, J., K. Dethloff, J. A. Francis, R. J. Hall, E. Hanna, S.-J. Kim, J. A. Screen, T. G. Shepherd, and T. Vihma (2016), Nonlinear response of mid-latitude weather to the changing Arctic, *Nat. Clim. Change*, *6*(11), 992–999.
Park, H.-S., S. Lee, S.-W. Son, S. B. Feldstein, and Y. Kosaka (2015), The impact of poleward moisture and sensible heat flux on arctic winter sea ice variability*, *J. Clim.*, *28*(13), 5030–5040.
Park, T.-W., C.-H. Ho, and S. Yang (2011), Relationship between the Arctic Oscillation and cold surges over East Asia, *J. Clim.*, *24*(1), 68–83.
Petoukhov, V., and V. A. Semenov (2010), A link between reduced Barents-Kara sea ice and cold winter extremes over northern continents, *J. Geophys. Res.*, *115*, D21111, doi:10.1029/2009JD013568.
Reynolds, R. W., T. M. Smith, C. Liu, D. B. Chelton, K. S. Casey, and M. G. Schlax (2007), Daily high-resolution-blended analyses for sea surface temperature, *J. Clim.*, *20*(22), 5473–5496.
Rigor, I. G., J. M. Wallace, and R. L. Colony (2002), Response of sea ice to the arctic oscillation, *J. Clim.*, *15*(18), 2648–2663.
Roeckner, E., G. Bäuml, L. Bonaventura, R. Brokopf, M. Esch, M. Giorgetta, S. Hagemann, I. Kirchner, L. Kornblueh, and E. Manzini (2003), The atmospheric general circulation model ECHAM 5. Part I: Model description.
Saha, S., et al. (2014), The NCEP Climate Forecast System Version 2, *J. Clim.*, *27*, 2185–2208, doi:10.1175/JCLI-D-12-00823.1.
Screen, J. A. (2017), Climate science: Far-flung effects of Arctic warming, *Nat. Geosci.*, doi:10.1038/ngeo2924.
Screen, J. A., and I. Simmonds (2013), Exploring links between Arctic amplification and mid-latitude weather, *Geophy. Res. Lett.*, *40*, 959–964, doi:10.1002/grl.50174.
Serreze, M., A. Barrett, J. Stroeve, D. Kindig, and M. Holland (2009), The emergence of surface-based Arctic amplification, *Cryosphere*, *3*(1), 11–19.
Tanaka, H., and H. Tokinaga (2002), Baroclinic instability in high latitudes induced by polar vortex: A connection to the Arctic Oscillation, *J. Atmos. Sci.*, *59*(1), 69–82.
The Weather Channel (2016), Winter Storm Jonas rivals biggest east coast snowstorms on record, Winter News. [Available at https://weather.com/storms/winter/news/east-coast-snowstorm-may-be-historic-2016].
Thompson, D. W., and J. M. Wallace (1998), The Arctic Oscillation signature in the wintertime geopotential height and temperature fields, *Geophy. Res. Lett.*, *25*, 1297–1300, doi:10.1029/98GL00950.
TIME (2016), East Asia hit by record snowfalls and cold weather (Jan 24, 2016), TIME. [Available at http://time.com/4192220/weather-east-asia-taiwan-japan-cold-winter/].
Trenberth, K. E. (1986), An assessment of the impact of transient eddies on the zonal flow during a blocking episode using localized Eliassen-Palm flux diagnostics, *J. Atmos. Sci.*, *43*(19), 2070–2087.
Tripathi, O. P., M. Baldwin, A. Charlton-Perez, M. Charron, S. D. Eckermann, E. Gerber, R. G. Harrison, D. R. Jackson, B. M. Kim, and Y. Kuroda (2015), The predictability of the extratropical stratosphere on monthly time-scales and its impact on the skill of tropospheric forecasts, *Q. J. R. Meteorol. Soc.*, *141*(689), 987–1003.
Vihma, T. (2014), Effects of Arctic sea ice decline on weather and climate: A review, *Surv. Geophys.*, *35*(5), 1175–1214.
Wang, J., and M. Ikeda (2000), Arctic oscillation and Arctic sea-ice oscillation, *Geophy. Res. Lett.*, *27*, 1287–1290, doi:10.1029/1999GL002389.
Wang, S.-Y., R. R. Gillies, and H. Dool (2014), On the yearly phase delay of winter intraseasonal mode in the western United States, *Clim. Dyn.*, *42*(5–6), 1649–1664.
Yoo, C., S. Lee, and S. B. Feldstein (2012), Mechanisms of Arctic surface air temperature change in response to the Madden-Julian Oscillation, *J. Clim.*, *25*(17), 5777–5790.